

# Calculated electron paramagnetic resonance $g$ -tensor and hyperfine parameters for zinc vacancy and N related defects in ZnO

Klichchupong Dabsamut<sup>a,b,\*</sup>, Adisak Boonchun<sup>b</sup>, and Walter R. L. Lambrecht<sup>a†</sup>

<sup>a</sup> *Department of Physics, Case Western Reserve University,  
10900 Euclid Avenue, Cleveland, Ohio 44106-7079, USA and*

<sup>b</sup> *Department of Physics, Faculty of Science, Kasetsart University, Bangkok 10900, Thailand*

Various defects in ZnO, focused on substitutional N<sub>O</sub> and N<sub>2</sub> in various sites, O-site, interstitial and Zn-site are studied using first-principles calculations with the goal of understanding the electron paramagnetic resonance (EPR) center reported for N<sub>2</sub> in ZnO and substitutional N on the O-site. The  $g$  tensors are calculated using the gauge including projector augmented wave (GIPAW) method and compared with experiments. The  $g$ -tensor of the free N<sub>2</sub><sup>+</sup> and N<sub>2</sub><sup>-</sup> radicals and their various contributions within the GIPAW theory are analyzed first to provide a baseline reference for the accuracy of the method and for understanding the N<sub>2</sub> behavior in ZnO. Previous controversies on the site location of N<sub>2</sub> in ZnO for this EPR center and on the shallow or deep nature and donor or acceptor nature of this center are resolved. We find that the N<sub>2</sub> on the Zn site is mostly zinc-vacancy like in its spin density and  $g$ -tensor, while for the O-site, a model with the N<sub>2</sub> axis lying in-the basal plane and the singly occupied  $\pi_g$ -orbital along the  $c$  axis provides good agreement with experiment. For the interstitial location, if the N<sub>2</sub> is not strongly interacting with the surroundings, no levels in the gap are found and hence also no possible EPR center. The calculated  $g$ -tensors for N<sub>O</sub> and V<sub>Zn</sub> are also found to be in good agreement with experiment. The effects of different functionals affecting the localization of the spin density are shown to affect the  $g$ -tensor values.

## I. INTRODUCTION

Electron Paramagnetic Resonance (EPR) provides one of the most powerful methods to study defect electronic structure. The  $g$ -tensor which describes the spin-splitting of a defect level in a magnetic field as function of the magnetic field magnitude and direction provides a unique fingerprint for the defect. Along with the hyperfine tensor, which describes the interaction with nuclear spins associated with the defect, the chemical identity of a defect can readily be determined. In combination with optical or thermal excitation or quenching of the EPR center, information on the defect levels can be obtained. However,  $g$ -tensors are rarely calculated from first-principles. Defects are usually described in periodic boundary conditions and it is only fairly recently that the methodologies for calculating  $g$ -tensors were developed for periodic systems. It requires calculating the induced current response to an external magnetic field or the orbital magnetization. This nontrivial problem was first solved for nuclear magnetic resonance (NMR) chemical shielding factors by including the gauge induced changes in the phases of the wave function in work by Mauri *et al.* [1, 2]. Subsequently, Ziegler and coworkers developed these approaches in the context of atom centered basis sets [3, 4] and Mauri *et al.* developed an implementation in terms of the projector augmented wave methods,[5, 6] known as the GIPAW (gauge including projector augmented wave) method. More recently, Ceresoli developed a non-perturbative approach based on Berry phases[7]

and also further improved the GIPAW code. The GIPAW method was applied to a number of defect systems by Gerstmann *et al.* [8–10] and Skachkov *et al.* [11–13]. These works illustrate the capability of the combination of theory and experiment in EPR to distinguish various defect models for a given EPR center.

Here we apply the GIPAW method to the study of several defects in ZnO. Our initial motivation was the work by Garces *et al.* [14] identifying N<sub>2</sub> in ZnO. They identified N<sub>2</sub> unequivocally on the basis of the characteristic hyperfine interaction with two  $I = 1$  N nuclei and hypothesized that the N<sub>2</sub> occurred on an O-site. They found an axially symmetric  $g$ -tensor with the symmetry axis along the  $c$ -axis of the wurtzite structure of ZnO. Subsequently, a computational study by Boonchun and Lambrecht[15] proposed instead a Zn-vacancy location for the N<sub>2</sub> based on the fact that the  $g$ -tensor agrees more closely with that of a N<sub>2</sub><sup>+</sup> radical than that of a N<sub>2</sub><sup>-</sup> radical. In fact, when N<sub>2</sub> sits on a Zn-site, it behaves as double acceptor with the 10 valence electrons of N<sub>2</sub> compared to the 12 valence electrons of Zn (including the filled 3d shell). The N<sub>2</sub> molecule, which then plays the role of a 2+ ion, would miss two electrons from its HOMO (highest occupied molecular orbital)  $\sigma_{g+}$  level. The  $q = -1$  state of the defect then corresponds to the singly occupied  $\sigma_{g+}$  state (or a N<sub>2</sub><sup>+</sup> radical) and is EPR active. The  $g$ -tensor of this N<sub>2</sub><sup>+</sup> radical was calculated by Bruna and Grein[16] and is characterized by a negligible  $\Delta g_{\parallel}$ -shift from the free electron value in the direction parallel to the bond and negative  $\Delta g_{\perp}$  in the direction perpendicular to the bond. This is readily understood in terms of second-order perturbation theory in which the  $\Delta g$ -tensor arises from the cross effect of spin-orbit coupling and the orbital Zeeman effect and can be written

\* klichchupong.d@gmail.com

† walter.lambrecht@case.edu

as

$$\Delta g_{ij} = 2\lambda \sum_n \frac{\langle 0|L_i|n\rangle\langle n|L_j|0\rangle}{E_0 - E_n}, \quad (1)$$

where  $\lambda$  is the atomic spin-orbit coupling,  $|0\rangle$  is the singly occupied molecular orbital (SOMO) whose spin splitting we try to calculate and  $|n\rangle$  are the other states with energy  $E_0$  and  $E_n$  respectively and,  $L_i$  and  $L_j$  are the cartesian components of the angular momentum operator. Since the angular momentum matrix elements from the SOMO  $\sigma_{g+}$  state can here only couple to the higher lying  $\pi_g$  LUMO (lowest unoccupied molecular orbital) for the components perpendicular to the axis of the molecule, this gives a negative contribution to the  $\Delta g_{\perp}$  as was indeed observed in the work of Garces *et al.* [14]. Boonchun and Lambrecht estimated this  $\Delta g_{\perp}$  for the  $N_2$  molecule using a tight-binding model for the  $N_2$  molecule with parameters fitted to density functional theory (DFT) calculation and using a calculated atomic spin-orbit coupling parameter to be  $-2600$  ppm in excellent agreement with Bruna and Grein's [16] calculation which gave a value of  $-2734$  ppm. Both are in good agreement with the angular average of  $\Delta g$  which amounts to  $\sim (2/3)\Delta g_{\perp}$  and experimentally is about  $-1900$  ppm. The latter calculation was based on a more advanced quantum chemical calculation of the molecular levels but used a similar perturbation theoretical approach.

On the other hand, on an O-site one would expect the  $N_2$  molecule to behave as a donor with an additional electron in the  $\pi_g$  state of the molecule, which then becomes a  $N_2^-$  radical. One then would expect a positive  $\Delta g_{\perp}$ -tensor within the same type of perturbation theory, as we'll show explicitly later in Sec. III A. The  $g$ -tensors of  $N_2^-$  on anion sites in MgO and KCl and other ionic compounds are well-known [17]. They are a bit more complex because the crystal environment breaks the degeneracy of the  $\pi_g$  state [17]. The main argument of Boonchun and Lambrecht [15] was that the  $g$ -tensors of  $N_2$  occurring on anion sites in these crystals differs significantly from that observed by Garces *et al.* [14]. However, in retrospect, it seems somewhat inconsistent that to explain the size of the hyperfine splitting one needs to assume a significant delocalization of the spin density beyond the molecule while for the  $g$ -tensor these models focused exclusively on the isolated molecule. Also, besides spin-orbit and orbital Zeeman perturbations, the full theory of  $g$ -tensors as implemented in the GIPAW code includes additional contributions, such as the spin-other-orbit terms which involve the magnetic field induced by the first-order induced current, diamagnetic contributions and so on. It seems worthwhile applying this method to re-evaluate the  $g$ -tensor for  $N_2$  in ZnO.

The proposal by Boonchun and Lambrecht [15] that  $N_2$  on Zn would be a relatively shallow acceptor was exciting because this could potentially lead to a path to the  $p$ -type doping of ZnO, which remains a challenging problem till today [18, 19]. However, their proposal was challenged in several ways. Petretto and Bruneval [20] found that

the  $N_2$  in the neutral state prefers to make a bridge type bond to two of the surrounding O atoms while the  $q = -1$  state of this molecule prefers the isolated site similar to the calculation of Boonchun and Lambrecht. However, this much lower energy of the  $N_2$  neutral state than leads to a much deeper  $0/-$  transition level making the system a deep rather than shallow acceptor. Furthermore they showed that energetically  $N_2$  prefers the O site over the Zn-site. Earlier, Nickel and Gluba [21] found several  $N_2$  interstitial sites in ZnO to have lower energy than on the O-site.

The claim of a shallow acceptor behavior of  $N_2$  in ZnO was also challenged by an experimental study by Phillips *et al.* [22] which studied the recharging behavior of the EPR active state. This study like Garces *et al.* [14] found that upon irradiation with light, above a critical phonon energy of about  $1.9$  eV a new signal identified with  $N_O$  becomes activated but unlike the Garces *et al.* study it also found the  $N_2$  signal to increase already at  $1.4$  eV while Garces *et al.* found irradiation to quench the EPR signal of  $N_2$ . To explain this, they proposed that their sample could be inhomogeneous with different Fermi level positions in different regions of the sample placing the Fermi level close to the defect level of the  $N_2$ , whereby not all  $N_2$  centers would originally be in the EPR active state. They associate the  $1.4$  eV activation energy with a transition from the defect to the conduction band and thus concluded the levels were deep. While they do not explicitly discuss which site the  $N_2$  is located on, this also suggests that the EPR active state is in a positive charge state because it requires removing an electron from the defect to the conduction band, and hence that  $N_2$  in ZnO is donor like. That would, in fact, correspond to Garces *et al.* [14]'s proposal. However, alternative explanations for the recharging behavior could still be possible and an explanation for the  $g$ -tensor itself is lacking.

From the above it is clear that several open questions remain on  $N_2$  in ZnO. This makes it worthwhile to revisit the  $N_2$  calculations in different sites, O, interstitial and Zn and explore whether different orientations of the molecule can occur. Calculating the  $g$ -factors should help to identify which of these various possible models corresponds to the experimental EPR signal and the corresponding energy levels at the hybrid functional level can be compared with experiment. To complement this study we also calculate the  $N_O$   $g$ -tensor. We start from first-principles calculations for both the  $N_2^-$  and  $N_2^+$  molecules and compare these with previous calculations as a test of the accuracy of the method.

As we will show, only the  $N_2$  on the O site originally proposed by Garces *et al.* [14] has a clear spin localization on the  $N_2$  molecule. The other systems have spin densities mostly on surrounding O atoms or very delocalized spin density. This suggests that the  $N_2$  on Zn-site electronic structure is closely related to the  $V_{Zn}$ . We thus also calculate the  $g$ -factor for the Zn-vacancy, for which also experimental data are available. Good agreement with these experimental  $g$ -tensor data is established. For

the interstitial location, in models in which the  $N_2$  minimally perturb the system, we find no levels in the gap and hence the  $+$  charge state corresponds to removing charge from the valence band maximum, leading to a very delocalized spin density and  $g$  tensors not compatible with the experimental data for  $N_2$  in ZnO.

We will show that the  $N_2$  on O site can explain qualitatively the data if we assume that the experiment measures some unresolved average over different symmetry equivalent orientations of the defect. The results are also sensitive to the density functional used as discussed in the computational methods section. We also calculate the  $g$ -factor for the substitutional N on O case and find reasonable agreement assuming again some degree of averaging occurs in the experiment. These results indicate that it might be possible to further resolve these EPR signals into separate centers corresponding to different orientations of the electronic structure on symmetry equivalent orbitals in future work, perhaps using higher magnetic fields and microwave frequencies to improve the resolution.

## II. COMPUTATIONAL METHOD

The initial defect relaxations are carried out at the hybrid functional level using a parametrized Heyd-Scuseria-Ernzerhof (HSE) potential [23, 24] in which the fraction of exact exchange  $\alpha$  is set to 0.375 and the standard screening length  $\mu = 10$  Å is used to cut off the long-range part of exact exchange. The relaxation calculations were carried out using the VASP code.[25–28] using well converged plane wave cut-off energy (500 eV) in the projector augmented wave (PAW)[29] method. Supercells of 128 atoms were used to model the defects.

Unfortunately, the GIPAW code has not yet implemented hybrid functionals but can since recent improvements include Hubbard-U terms. It is integrated with the QUANTUM ESPRESSO (QE) code [30] which provides similar functionality to the VASP code. After determining the self-consistent potential of the system with a standard QE run, the GIPAW code evaluates the first-order induced current using density functional perturbation (DFPT) and from this extracts various  $g$ -tensor contributions, including the magnetic field induced by the first-order current from the Biot-Savart law, which leads to the spin-other-orbit contributions. It also includes other relativistic corrections besides spin-orbit coupling and distinguishes paramagnetic and diamagnetic contributions as explained in detail in Ref. 5 and 6. For most of the  $g$ -tensor calculations we use the generalized gradient approximation (GGA) in the Perdew-Burke-Ernzerhof (PBE) parametrization [31] but at the atomic positions relaxed with hybrid functional. In some cases we also used Hubbard-U corrections to the PBE functional which can simulate the hybrid functional effects in creating an orbital dependent potential with stronger hole localization. We checked that the hybrid functional with the

TABLE I.  $\Delta g$ -tensor of  $N_2^+$  radical in ppm: comparison with other calculations and contributions to GIPAW (PBE) as detailed in Ref. [6]

contribution	$\Delta g_{\parallel}$	$\Delta g_{\perp}$
total GIPAW (PBE)	-121	-3180
total GIPAW (PBE+U)	-125	-3126
total Bruna <sup>a</sup>	-249	-2734
total TB model <sup>b</sup>	0	-2600
relativistic mass	-259	-259
SO bare	49	-704
SO para	0.2	-2271
SO dia	8	12
SOO	81	42

<sup>a</sup> Bruna and Grein[16]

<sup>b</sup> Boonchun and Lambrecht[15]

parameters used here, satisfy the generalized Koopmans' theorem [32–35] quite well for all of the defects considered here and at the same time provide an accurate band gap of 3.4 eV. Details about these tests are given in Supplemental Material[36]. We use these calculations to evaluate defect transition levels using the standard defect formation energy formalism as outlined in Freysoldt *et al.* [37] and to determine the structural models of the defects.

These same relaxed structures are then used to calculate  $g$ -tensors either in PBE or in PBE+U. Adding Hubbard-U terms to adjust to hybrid functional results is not trivial. One has several choices: adding  $U$  on Zn- $d$ , O- $p$  and N- $p$ . Our aim is not to provide a fully optimized choice but to gain insight in qualitative effects of adding specific  $U$  terms.

Hyperfine tensors were also calculated using the GIPAW code. They make use of the PAW reconstruction of the full atomic wave function including relativistic corrections.[38–40]

## III. RESULTS

### A. $N_2$ radicals

#### 1. $g$ -tensors

We start with the results for the  $g$ -tensors of the  $N_2$  molecule in the  $+1$  and  $-1$  charge states as shown in Table I, II. We can see from the table that the dominant contributions to the  $\Delta g_{\perp}$  are the spin-orbit (SO) paramagnetic and bare term. The bare term refers to the pseudo part of the wave function and the paramagnetic part corresponds to the PAW reconstructed parts of the full atomic wavefunction. The diamagnetic and spin-other-orbit (SOO) contributions are small. The agreement with the other calculations which use a much simpler approach is excellent. The Bruna and Grein approach [16] calculates first-order contributions to  $\Delta g$  at

TABLE II. Calculated  $\Delta g$  (in ppm) terms for  $N_2^-$  using the GIPAW approach.

contribution	$\Delta g_{\parallel}$	$\Delta g_{\perp}$
total GIPAW	53	1741
relativistic mass	-2	-2
SO bare	14	447
SO para	41	1296
SO dia	0.1	0.1
SOO	-0.2	-0.4

the realistic open-shell Hartree-Fock level and the second order terms correspond to the cross terms of orbital Zeeman and spin-orbit coupling, essentially as in Eq.(1). In the GIPAW approach the relativistic mass term and diamagnetic terms are also first-order terms in the sense that they are calculated from expectation values using the zero-th order wave functions. The SOO and SO para and bare term terms are second order corrections to the energy since they involve first-order wave functions. Thus, the sum of SO dia and relativistic mass corrections should be compared with the Bruna value for the  $\Delta g_{\parallel}$ . The orientation averaged  $\Delta g$  in our present GIPAW calculation is  $-2160$  ppm and is close to the experimental value of  $-1900$  as reported in Bruna and Grein [16]. The above values were obtained in PBE. When adding a  $U$  on  $N$ - $p$  orbitals of 3 eV, the values change slightly. We only report the decomposition in partial contributions for the PBE case. The decomposition is similar with the SO diamagnetic mass corrections and SOO almost unchanged and the differences arising mostly from the SO paramagnetic and bare terms which indeed depend on energy level splittings because they are second-order corrections to the energy. This calculation provides a good benchmark for the accuracy of the GIPAW approach.

For the  $N_2^-$  radical we find again that the dominant contribution are the paramagnetic and bare SO terms. They are positive in this case and this is easy to understand from the Eq.(1) since now the unpaired spin is in the  $\pi_g$  state and it can give non-zero off-diagonal matrix elements of the angular momentum operator with two lower lying  $\sigma_g$  states. In this calculation, we have occupied one of the degenerate  $\pi_g$  states and thereby broken the symmetry in our spin-polarized DFT calculation. This confirms that the  $N_2^+$  and  $N_2^-$  radicals have opposite signs of the main  $\Delta g_{\perp}$ . Of course these results correspond to the isolated molecule and this may change when the molecule is placed in a crystal environment and other levels of the system become involved.

## 2. Hyperfine tensors

The hyperfine tensor for the diatomic molecule contains a dipole part which is axial with parameters  $A_{\perp} = A_{dip}$ ,  $A_{\parallel} = -2A_{\perp}$  and the isotropic Fermi contact term  $A_{iso}$ . Our calculated values compared to experiment and

TABLE III. Hyperfine tensor parameters for  $N_2^+$  and  $N_2^-$  in MHz.

	$A_{dip}$	$A_{iso}$
	$N_2^+$	
This work PBE	-30.4	102.2
This work PBE+ $U$	-29.9	95.6
Expt	23.3	102.4 <sup>a</sup>
		104.1 <sup>b</sup>
Other calc.	29.7	91.3 <sup>c</sup>
	$N_2^-$	
This work PBE	-0.14	2.92
This work PBE+ $U$	-0.13	2.99

<sup>a</sup> Scholl *et al.* [41]

<sup>b</sup> Knight *et al.* [42]

<sup>c</sup> Bruna and Grein [16]

other calculations are given in Table III.

Note that the experiment does not detect the sign of the hyperfine tensor. The agreement is quite good. The Fermi contact term depends slightly on the functional. Interestingly, while adding  $U$  is expected to make the wave function more localized, its Fermi contact term nonetheless slightly decreases. This must indicate that the  $s$ -component of the wave function is slightly decreased. Note that we included  $U$  on the  $N$ - $2p$ . Various other calculated results are reviewed in Bruna and Grein[16] and give a range of values with average  $88 \pm 10$  for the Fermi contact term. For the  $N_2^-$  radical, we find a much smaller hyperfine interaction. For the isotropic Fermi contact term, this is clearly related to that the unpaired spin in this case is in a  $\pi_g$  state and has no direct  $s$  contribution to the wave function.

## B. Zn-vacancy

### 1. $g$ -tensor

Next we consider the Zn-vacancy. Unconstrained relaxations carried out in hybrid functional led to a model in which the spin is clearly localized on a single O which moved away from the vacancy, thus forming a polaronic state. This can be seen in Fig. 1. In this case, it was localized on a lateral O in the basal plane next to the vacancy and thus the system has only  $C_s$  symmetry, containing only a mirror plane. The **a**, **b**, **c** vectors in this figure are the lattice vectors of the supercell and correspond to  $[01\bar{1}0]$ ,  $[\bar{2}110]$  and  $[0001]$  directions. Thus the spin density is seen to lie in a  $(\bar{2}110)$  plane and with the smallest ( $\Delta g < 0$ ) principal axis closer to the **c** axis. On the other hand, if the spin localizes on the axial O, the symmetry of the system remains  $C_{3v}$ . Experimentally both of these cases have been observed in the work of Galland and Herve [43] and the  $V_{Zn}$  EPR center was also studied by Son *et al.* [44], who identified a separate center with H attached to the O in the  $V_{Zn}$ . Here, we only



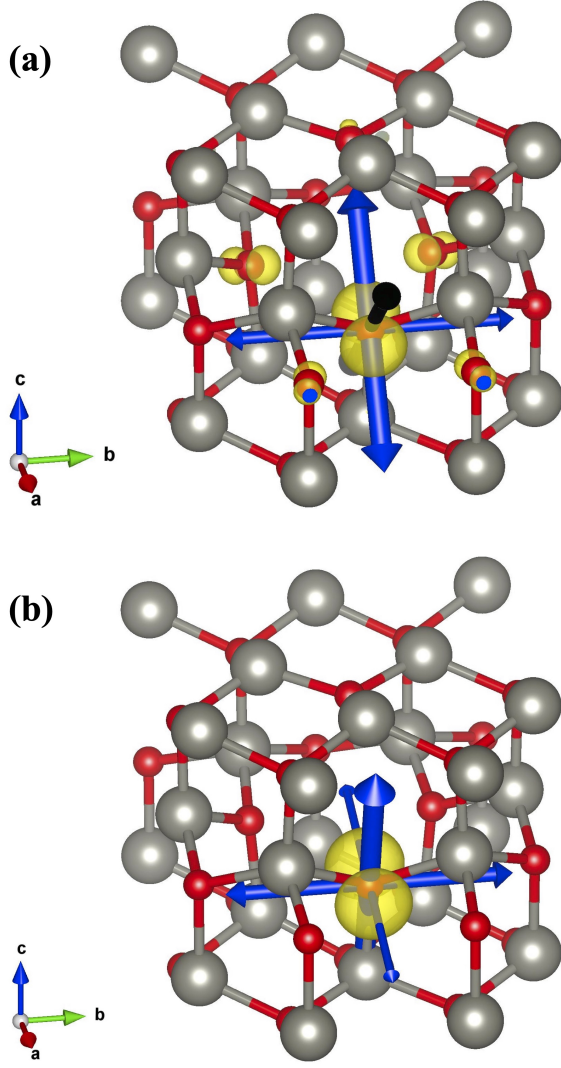


FIG. 1. Relaxed structure in (a) PBE and (b) PBE+U near the  $V_{\text{Zn}}$  in the EPR active  $q = -1$  charge state, showing the net spin density as a yellow isosurface. The double-sided vectors show the  $\Delta g$  tensor principal axes and the thickness of vectors indicate how big the magnitude of  $|\Delta g|$  is, black and blue represents negative and positive values, respectively.

discuss the  $V_{\text{Zn}}$ . The  $g$ -tensor and its principle axes are given in Table IV.

We can see that in the experiment, the smallest  $g$  component is still larger than the free-electron value  $g_e = 2.002319$  and has its principle axis at  $69.25^\circ$  from the  $c$  axis in a  $\langle 1\bar{2}10 \rangle$  plane, which is a mirror plane of the wurtzite structure. Note that the opposite direction is  $111^\circ$  from the  $c$ -axis, which is close to the  $109^\circ$  ideal tetrahedral angle, which means that this direction is the direction of the broken Zn-O bond. Thus, as usual the lowest  $\Delta g$  occurs is along the direction of the dangling bond. The two other principal values are close to each other and are larger and positive. This is also consistent

TABLE IV.  $g$ -tensor and principle axes for the  $V_{\text{Zn}}$ .

	$g_1$	$g_2$	$g_3$
Expt. <sup>a</sup>	2.0028	2.0173	2.0183
principle axes	$\theta_c = 69.25^\circ$	$\theta_c = 20.75^\circ$	
	in $\langle 1\bar{2}10 \rangle$		$\perp \langle 1\bar{2}10 \rangle$
Calc PBE	1.9948	2.0166	2.0096
principle axes	$\theta_c = 38^\circ$	$\theta_c = 52^\circ$	
	in $\langle 1\bar{2}10 \rangle$		$\perp \langle 1\bar{2}10 \rangle$
Calc PBE+U	2.0039	2.0095	2.0092
principle axes	$\theta_c = 73^\circ$	$\theta_c = 17^\circ$	
	in $\langle 1\bar{2}10 \rangle$		$\perp \langle 1\bar{2}10 \rangle$

<sup>a</sup> Galland and Herve [43]

with the  $C_{3v}$  center with the hole localized on the axial O in which case the expt. values are  $g_{\parallel} = 2.0024$  and  $g_{\perp} = 2.0193$ . Comparing to the PBE calculated values, we see the  $g$ -tensor still lies in a  $\langle 1\bar{2}10 \rangle$  plane but the smallest value is now negative and at  $38^\circ$  or  $142^\circ$  from the  $c$ -axis. Adding a Hubbard- $U$  term of 5 eV on the O- $p$  orbitals makes this  $\Delta g$  positive, but overshoots slightly compared to experiment. The angle  $\theta_c$  from the  $c$ -axis is now  $73^\circ$ , or  $107^\circ$ , much closer to the experiment and to the dangling bond direction. The wave function also become more localized exclusively on this one O (as shown in Fig. 1(b), while in PBE it had some small components on the other two lateral O neighbors of the Zn-vacancy. This is as expected from DFT+U in which the  $U$  terms tends to make the spin density more localized by pushing the hole state deeper into the gap. The principal values in the directions perpendicular to the dangling bond are smaller than in experiment but indeed larger than along the dangling bond and closer to each other than in the PBE case. Using a smaller value of  $U = 3$  eV give  $g_1 = 2.0054$ ,  $g_2 = 2.0117$  and  $g_3 = 2.0128$ , giving a larger overestimate of the small  $g_1$ , which we might call  $g_{\parallel}$  (meaning parallel to the dangling bond) and larger values for  $g_2$  and  $g_3$  which we might average to  $g_{\perp}$ , which are closer to experiment. Further inspection of the  $\Delta g$  contributions shows that the SOO contribution is small and increasing  $U$  increased the paramagnetic SO contribution for both parallel and perpendicular directions. Adding a  $U_d = 6$  eV on Zn- $d$  and  $U_p = 3$  eV on O- $p$  reduced  $g_{\parallel}$  to 2.0036 but also reduced  $g_{\perp}$  to 2.0097. The directions of the principal axes barely changed.

These results confirm the basic model proposed by Galland and Herve [43], who analyzed the  $\Delta g$  tensor essentially based on Eq.(1) and viewed it as originating from the splitting between the O- $p$  state on which the hole is localized from its perpendicular directions. Since the hole is a localized O- $p$  type dangling bond, it lies above the other O- $p$  states and the SO contribution to  $\Delta g$  is thus positive for  $g_{\perp}$  and negligible for  $g_{\parallel}$  in their model. The full calculation indicates that the  $\Delta g_{\parallel}$  is not exactly zero and also slightly positive. The details depend obviously sensitively on the degree of localization of the wave function. All the models considered here including  $U$  give

TABLE V.  $g$ -tensors for  $\text{N}_\text{O}$ .

Expt. <sup>a</sup>	$g_{\parallel c}$	$g_{\perp c}$	
	1.995	1.963	
	$g_{\parallel}$	$g_c$	$g_{\perp}$
PBE	2.0093	1.9810	1.9843
principal axes	$\theta_b = 27^\circ$	$\theta_c = 36^\circ$	$\theta_a = 36^\circ$
PBE+ $U_{\text{Np}} = 3$ eV	2.0062	2.0014	2.0029

<sup>a</sup> Phillips *et al.* [22]

better results than the pure PBE results because the latter has a wave function too delocalized on other nearby O next to the vacancy even though we already created some difference between the three lateral O by relaxing the structure within hybrid functional.

Our HSE and PBE+U calculations show that the defect transition levels for  $V_{\text{Zn}}$  are 1.38 and 0.29 eV, respectively. The HSE results agrees with previous studies of 1.4 eV[45, 46]. The PBE+U gives a significantly less deep level, consistent with previous research which gives values ranging 0.17–0.3 eV[47–49].

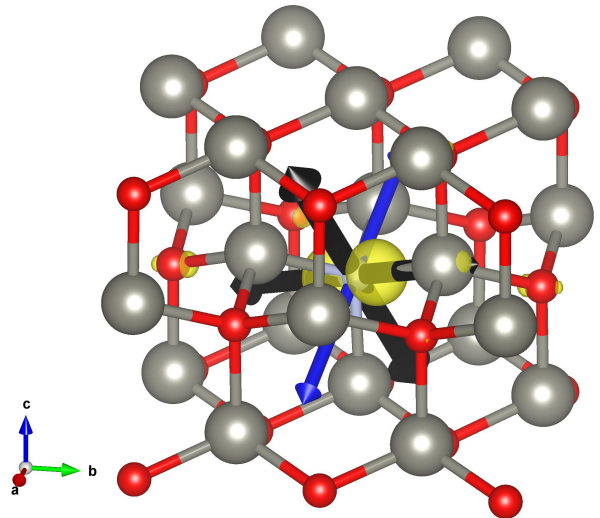
## 2. Hyperfine

For the  $V_{\text{Zn}}$  the spin localizes on a single oxygen. Oxygen has only isotope  $^{17}\text{O}$  with non-zero nuclear spin  $I = 5/2$  and this isotope has only 0.038 % natural abundance. Nonetheless, calculating it gives a value of  $A_{\text{dip}} = 74$  MHz and  $A_{\text{iso}} = 27$  MHz on the oxygen on which the spin is localized.

For Zn there is one isotope  $^{67}\text{Zn}$  with spin  $I = 5/2$  which has 4.10 % abundance. We find non-negligible Fermi contact terms hyperfine on only three of the Zn atoms in the cell, namely the three that are nearest neighbors to the oxygen on which the spin is localized. Their hyperfine tensors  $A_{\text{iso}}$  range from -13.7 to -16.7 MHz. The dipolar parts  $A_{\text{dip}} \approx 1$  MHz.

## C. Substitutional N on O-site

Next, we turn our attention to the substitutional  $\text{N}_\text{O}$  case. This is a well studied defect and found to have a very deep 0/- level. The results from our HSE calculation of 2.02 eV is a bit deeper than previously obtained values [15, 50]. However, our PBE+U functional is 0.56 eV while LDA calculation reported this value of 0.4 eV [51]. The spin density of the neutral charge state is shown in Fig. 2. The  $g$ -tensor is compared with experiment in Table V. The unconstrained relaxation gave a spin density localized mostly on N on a  $p$ -orbital approximately along the  $b$  direction ( $[\bar{2}110]$ ) and with small contributions on various second neighbor O atoms, as can be seen in Fig. 2. In the experiment the  $g_{\parallel}$  corresponds to the  $c$ -axis and if fully axially symmetric while we find a higher anisotropy. At first, one might assume

FIG. 2. Spin density for  $\text{N}_\text{O}$  in the neutral charge state and EPR  $g$ -factor.

that this just means that the spin became localized on a  $\text{N-}p_z$  orbital along the  $c$  axis in the experiment. However, we may also assume that the experiment sees an average of centers with spin localized in the basal plane and along  $c$ . Also, our  $\Delta g_{\parallel} = 6981$  ppm is positive while the experimental value is negative. For our calculations  $g_{\parallel}$  indicates parallel to the unpaired spin orbital,  $g_{\perp}$  indicates in the basal plane perpendicular to the spin orbital and  $g_c$  indicates along the  $c$  axis. Averaging the values in the  $c$  direction, assuming three equivalent in the basal plane orientations and one along the  $c$  axis, we can write  $\bar{g}_c = (g_{\parallel} + 3g_c)/4$  which gives a value of 1.988. For the direction perpendicular to  $c$  we can write  $\bar{g}_{\perp c} = [(g_{\parallel} + g_{\perp})3/2 + (g_c + g_{\perp})/2]/4 = 1.993$ . This gives two negative  $\Delta g$  values close to each other as in the experiment but fails to capture the small difference between in the basal plane and along  $c$  observed in the experiment. There might be some energetic advantage to the spin localizing in the  $c$  direction which would then explain the smaller negative value in the  $c$  direction. Adding  $U$  values of 3 eV or 5 eV on N or both on N and O did not change the orientation of the spin density nor its degree of localization. It tends to make the  $\Delta g$  values closer to each other and smaller but no improvement with the experimental values was obtained.

It was found experimentally[22] that the  $\text{N}_\text{O}$  center is activated by light of about 1.9 eV. We have thus calculated the vertical transitions energy from the negative charge state to the neutral one plus an electron at the conduction band minimum. Including only the image charge correction to the negative charge state, we obtain 1.98 eV for this activation. However, recently, it was proposed[52] that even the neutral charge state in the frozen geometry of the negative charge state requires a correction due to the presence of polarization charge and

this needs be screened using only the electronic screening. This gives 2.25 eV. Both are in reasonable agreement with the experiment.

As for the hyperfine tensor for  $\text{N}_2$ , we find  $A_{iso} = 24$  MHz and  $A_{dip} = -27$  MHz on the N atom with the  $A_{||} = -2A_{dip}$  along the  $\mathbf{c}$  axis. Thus, we obtain  $A_{||c} \approx 78$  and  $|A_{\perp c}| \approx 3$  MHz. Phillips *et al.* [22] give values of  $A_{||c} = 81$  and  $A_{\perp c} = 8.5$  MHz. These values are in fair agreement.

## D. $\text{N}_2$ in ZnO

### 1. Zn-site

First we considered various models for  $\text{N}_2$  placed inside the Zn-vacancy. One of our goals here is to revisit the question of whether the  $\text{N}_2$  in this site is a shallow or deep acceptor. We start from different initial orientations of the molecule, either parallel to  $\mathbf{c}$  or in the basal plane and in the basal plane either with the molecular axis pointing toward one of the neighboring O or perpendicular to it. We also started either from the ideal crystal or from the previously relaxed vacancy. To summarize these results, we found that the lowest energy for the neutral charge state has the  $\text{N}_2$  forming a bridge like bond along one of the tetrahedral sides surrounding the vacancy and connecting to two O atoms. This configuration, also reported by Petretto and Bruneval[20], has about 0.465 eV lower than the in-basal plane configuration with the molecule aligned with one of the bonds in which case it can still make a single N-O bond if we place it close to an O or can be essentially isolated. The vertically aligned molecule tended to flip back to a horizontal position or at least tilt slightly. We also shifted the center of gravity of this molecule up or down from the  $V_{\text{Zn}}$  center to keep it more isolated. On the other hand in the EPR active  $q = -1$  charge state the isolated  $\text{N}_2$  molecule had the lowest energy. The transition level ( $0/-$ ) is in principle calculated from the lowest energy configuration of each charge state and is then found to be 2.46 eV using the HSE functional which is considerably deeper above the valence band maximum than the shallow one of 0.17 eV obtained using PBE+U. These results support the conclusion of Petretto and Bruneval[20] and contradict those of Boonchun and Lambrecht[15], which did only consider a more isolated configuration of  $\text{N}_2$  and furthermore proposed that the generalized Koopmans' condition is better satisfied within PBE than PBE+U and thereby obtained a shallower defect level. Thus, our first conclusion here is that  $\text{N}_2$  on Zn site would be a deep acceptor. The figure of these structural models can be found in Supplemental Material[36].

Turning now to the spin densities, we find that the spin density showed very little contribution on the  $\text{N}_2$  mostly on a single O neighbor. This is shown in Fig. 3. The  $g$ -tensor is then similar to the  $V_{\text{Zn}}$  case with all positive  $\Delta g$  values. Again, if the spin was oriented for example

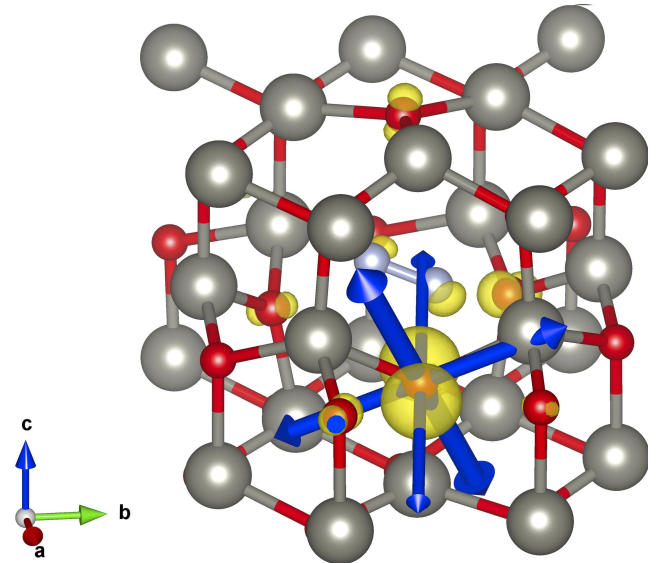


FIG. 3.  $\text{N}_2$  in  $V_{\text{Zn}}$  relaxed structure in the  $q = -1$  state with spin isosurface and  $g$ -tensor.

along the  $\mathbf{a}$  direction, then the lowest  $\Delta g$  principal value occurred along that direction. The  $\Delta g$  shifts are similar to that of the vacancy. These are very different from the values reported for  $\text{N}_2$  in ZnO by Garces *et al.* [14] and Phillips *et al.* [22] and we thus conclude that  $\text{N}_2$  on a Zn site is incompatible with the observed EPR center. Furthermore it implies that if  $\text{N}_2$  would be isolated in a Zn-vacancy it only slightly perturbs the vacancy and leads to a polaronic systems with spin localized on a single O as in the vacancy case.

### 2. Interstitial sites

Next we consider various interstitial sites. Among these, the lowest energy is obtained for the structure where  $\text{N}_2$  occurs in the middle of the large hexagonal interstitial site. We constrained this model so as to allow the molecule only to move along the  $z$  direction. It is shown in the Supplemental Material [36]. In this case, we found that the  $\text{N}_2$  molecular states are deep enough that the HOMO  $\sigma_{g+}$  state stays occupied and the  $\pi_g$  is empty. The neutral charge state shows no levels in the gap at all. Attempting to make a  $q = +1$  charge state then leads to removing an electron from the VBM resulting in a very delocalized spin density. The  $g$ -tensor calculated shows a very large negative values along the  $\mathbf{c}$  direction, about  $g_c = 1.7132$  and a value of about  $g_{\perp c} \approx 1.99$ . We think these may reflect the  $g$ -tensor of the VBM but additional work is needed to understand these values. The  $g$ -tensor of such delocalized states like the VBM or CBM are usually discussed in terms of  $\mathbf{k} \cdot \mathbf{p}$  theory.[53] We do not discuss it further here but rule out any of these sites as responsible for the observed  $\text{N}_2$  EPR center in ZnO. Although this does not refute that  $\text{N}_2$  could occur intersti-



TABLE VI.  $g$ -tensors for  $N_2$  on O-site

		$g_{\parallel N_2}$	$g_{\parallel \pi-orbital}$	$g_{\perp \pi-orbital}$
$N_2 \parallel c$	PBE	1.95378	1.98724	2.00007
	PBE+ $U^a$	1.98736	2.00381	2.00988
$N_2 \perp c$	PBE	1.98494	2.00506	2.00911
	PBE+ $U$	1.99281	2.00457	2.00666
		$g_{\parallel c}$	$g_{\perp c}$	
	Expt.	2.0036	1.9935	
$N_2 \perp c$	SOMO $\parallel c$	2.0038	1.9986 <sup>b</sup>	

<sup>a</sup>  $U = 3$  eV on N and O<sup>b</sup> average of columns 1 and 3 for row 2

tially as claimed by Nickel and Gluba[21], it presumably has no EPR active state in this case because no defect levels are found in the gap from which a singly occupied unpaired spin state can be constructed. Other interstitial forms of  $N_2$  may disrupt the ZnO network and hence lead to O dangling bond type states as reported by Nickel and Gluba[21] but they do not lead to an EPR center with spin density on the  $N_2$  molecule compatible with the one observed [14] and are thus not further pursued here.

### 3. O-site

Finally, we return to the  $N_2$  molecule in the O-site as initially proposed by Garces *et al.* [14]. We started out from an initial orientation of the molecular  $N_2$  bond axis parallel to the  $c$  axis. The  $N_2$  molecule was allowed to move only in  $c$  direction. After relaxation the spin density was strongly localized on the  $N_2$  molecule and shows clearly a  $\pi_g$  like state which happened to be oriented with the  $a$  axis. This is shown in Fig. 4(a). The defect in this case is a donor and the spin density corresponds to the  $q = +1$  charge state of the defect, which is, however, a  $N_2^-$  from the view of the  $N_2$  molecule. The defect transition level (+/0) for this case is 3.07 using HSE (1.46 eV in PBE+ $U$ ). We also investigate the  $N_2$  molecular with its bond axis perpendicular to the  $c$  axis. We start the configuration by pointing the  $N_2$  toward one of neighboring Zn as can be seen in Supplemental Material[36]. After the relaxation by fixing the molecule's movement in the  $z$  direction, the  $N_2$  molecule is pointing to the space between two Zn atoms. Like the previous model, the spin density was strongly localized on the  $N_2$ . The defect transition levels of this model, 3.23 and 1.59 eV using HSE and PBE+ $U$ , are somewhat deeper than those of  $N_2$  parallel to the  $c$  axis. Full unconstrained relaxation of the  $N_2$  molecule led to an orientation intermediate between these two cases.

The  $g$ -tensor for the  $N_2$  molecule parallel to the  $c$ -axis, is found to have the lowest principal value along the direction of the  $N_2$  axis and in fact has a negative  $\Delta g$  in this direction. The next higher  $g$ -principal value is in the direction of the  $\pi_g$  SOMO orbital and the highest value perpendicular to the plane of the molecular axis

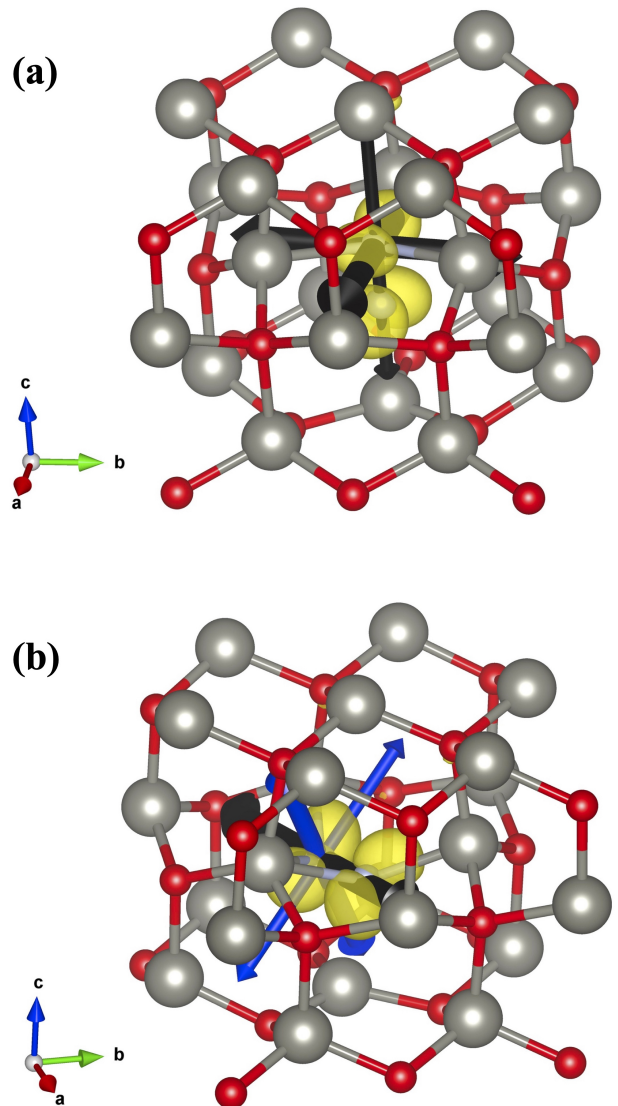


FIG. 4. Spin density and relaxed structure for  $N_2$  in the O-site with the molecular axis fixed (a) parallel and (b) perpendicular to the  $c$ -axis.

and the  $\pi$ -orbital. This corresponds to the first row in Table VI. We can see in rows 3-4 of the table that this is true also when the  $N_2$  axis is fixed to be perpendicular to  $c$ . In case of a full relaxation, we find some intermediate orientation. We do not find convincingly lower energy among any of these orientations, which in the end result in energies within the error bar from each other.

All values slightly increase if we add a Hubbard- $U$  on both N and O and this makes the two higher values correspond to a small positive  $\Delta g$  for the first case where  $N_2$  is parallel to the  $c$  axis. When we fix  $N_2$  to lie in the  $bc$  plane, we already obtain two positive and one negative  $\Delta g$  in PBE but the SOMO is not lying in the plane but is slightly tilted as shown in Fig. 4(b). There are thus small variations in these  $g$ -tensors with the functional and de-

TABLE VII. Hyperfine parameters (in MHz) on N for N<sub>2</sub> on O-site.

	atom	$A_{dip}$	$A_{iso}$
N <sub>2</sub>    <b>c</b> PBE	N <sub>1</sub>	(-28.5, -30.7, 59.2)	15.7
	N <sub>2</sub>	(-17.0, -19.9, 36.9)	6.3
N <sub>2</sub> ⊥ <b>c</b> PBE	N <sub>1</sub>	(-23.1, -23.6, 46.7)	14.6
	N <sub>2</sub>	(-23.4, -23.9, 47.3)	14.9

pending on the orientation of the molecule but the basic correlation between molecular axes, and the broken symmetry of the  $\pi_g$  orbital in which the hole resides stay consistent. Further inspection shows that, as usual, the mass correction, diamagnetic and SOO contributions are small. The main paramagnetic contribution is strongly negative both in the GIPAW and bare terms for the **c** direction while the paramagnetic GIPAW term is positive for the directions in the plane of the molecular axis and its spin orbital.

The  $g$ -tensor at first does not seem to agree with the experiment which has a  $g_{||c} = 2.0036$  and  $g_{\perp c} = 1.9935$ . However, let's now consider that the molecule might be oriented in various equivalent ways and that the experiment sees an unresolved average of these. We then have several possibilities, the molecular axis might be along **c** as in row 1 of Table VI or perpendicular to it with either the  $\pi$  orbital along **c**, or perpendicular to it, or somewhere in between as in the last two rows of the table. We obtain the following averages based on the  $g$ -tensors of row 2 of Table VI. For N<sub>2</sub> axis parallel to **c**:  $g_{||c} = 1.98736$ ,  $g_{\perp c} = 2.0068$ , for N<sub>2</sub> axis in the basal plane and the  $\pi$  orbital along **c**:  $g_{||c} = 2.00381$ ,  $g_{\perp c} = 1.9986$ , and finally for N<sub>2</sub> axis in the basal plane and the  $\pi$  orbital perpendicular **c**:  $g_{||c} = 2.00988$ ,  $g_{\perp c} = 1.99558$ . The first choice disagrees with experiment but both cases with the axis in the basal plane are compatible with the experimental value with a slightly better agreement if the  $\pi$ -orbital is along the **c** axis. In fact, in this case the agreement is pretty close. Furthermore, also in the two cases (row 3 and 4) where we explicitly constrained the molecular axis to be in the plane but found the SOMO to be tilted away from the plane, we find a negative  $\Delta g$  perpendicular to the plane along the molecular axis and the other two directions have positive  $\Delta g$  with the largest one in the direction perpendicular to the plane of the molecular axis and the SOMO orbital. This direction is found to be closest to the **c**-direction, about 30 ° away from it. We may deduced from this that the experimental data are compatible with a preferred orientation of the molecular axis in or close to the basal plane. The axial symmetry along **c** observed experimentally does not correspond to a simple orientation of the molecule along this axis but rather some average over various in-plane orientations of the molecule.

The activation energy of the EPR center of (N<sub>2</sub>)<sub>O</sub> corresponds to a transition from the neutral to the positive state releasing an electron to the conduction band mini-

mum. This vertical transition is calculated to be 1.57 eV for the case of the molecular axis being in plane and 1.72 eV for the vertically aligned molecular axis, following the approach of Falletta [52] for the correction terms, in other words, using here only electronic screening. These values are in reasonable agreement with the experimental observation that the EPR signal of the N<sub>2</sub> in ZnO is enhanced by light of already 1.4 eV, so somewhat lower by about 0.5 eV than the N<sub>O</sub> substitutional defect. Since we here found the N<sub>O</sub> calculated to have an activation energy of around 2.2 eV, this is qualitatively also in agreement with experiment.

Finally, we consider the hyperfine tensor for the N<sub>2</sub> on O site. We give the eigenvalues of the hyperfine dipolar tensor as three values in parentheses for each of the N atoms. For the N<sub>2</sub> || **c** case, the values on both atoms differ somewhat but their average value is still close to -23 MHz, which is also close to that of the isolated N<sub>2</sub><sup>+</sup> molecule. For the isotropic part, the value is about 10 times smaller than for the N<sub>2</sub><sup>+</sup> case. This could at first sight indicate significant delocalization of the defect wave function. However, what really matters for the Fermi contact term is the amount of N-*s* wave function. In fact, the values are significantly larger than those of the N<sub>2</sub><sup>-</sup> isolated radical. The wave function here is clearly not purely *p*-like on N even though it is related to a  $\pi_g$  state. The N-*p*-like part of the wave function is responsible for the dipolar part and the closeness to the values for the N<sub>2</sub><sup>+</sup> molecule indicate that the wave function is still strongly localized on the N<sub>2</sub>.

Comparing to experimental data by Garces *et al.* [14] and Phillips *et al.* [22], who give  $A_{||c} = 9.8$  and  $A_{\perp c} = 20.1$  MHz, we note that our value for  $A_{||N_2} = -8$  and  $A_{\perp N_2} = 62$  MHz. So, if the molecule lies in the plane  $|A_{||c}| = 8$  MHz and the  $|A_{\perp c}|$  is the average of these two or 27 MHz. These are consistent with the experimental values.

#### 4. Summary

We thus conclude that among the various models for N<sub>2</sub> in ZnO, only the O site gives possibly a  $g$ -tensor compatible with the experiment because it is the only model with spin density localized on the N<sub>2</sub> molecule. In order to obtain agreement we need to assume that the N<sub>2</sub> molecule tends to lie preferentially with its axis in the basal plane and most likely with the  $\pi$ -orbital containing the unpaired spin pointing in the **c** direction or close to it. In fact, there are three possible high-symmetry orientations in the plane with the molecular axis in a mirror plane vs. only one along **c** for the N<sub>2</sub> axis, so simply statistically, it is more likely to find planar orientation. We did not find a clear energy advantage for this orientation. They were all close and also close to the fully relaxed minimum energy orientation which was intermediate. Thus we assume that the experiment samples some average over these different orientation of the

molecule. The degeneracy of the  $\pi_g$  state is broken with one particular orientation of the orbitals containing the unpaired spin. Because the  $g$ -tensor in the direction of the bond is strongly negative, the dominant in-plane orientation of the molecular axis leads to an average negative  $\Delta g_{\perp c}$  value in agreement with experiment. The otherwise mostly positive  $\Delta g$  values are compatible with our initial calculation for the  $N_2^-$  radical and the largest positive value occurs for the direction perpendicular to the plane of the SOMO, which we found to be close the  $c$ -axis, thus explaining the positive  $\Delta g_{\parallel c}$  in the experiment. The negative value along the bond must arise somehow from the interplay with the crystal levels rather than from the molecule itself.

#### IV. CONCLUSIONS

In conclusion, we have carried out  $g$ -tensor calculations for isolated molecules of  $N_2$  radicals with one electron subtracted or added and analyzed the different contributions to it in the GIPAW theory and compared them to previous perturbation theory approaches. We have shown that the EPR signal of  $N_2$  in ZnO is only compatible with calculated  $g$  tensors for the O-site. In that case, the  $N_2$  behaves as a deep donor and this is compatible with the recharging studies of Phillips *et al.* [22]. For the Zn-site, the  $N_2$  molecule tends to bind to two O in the neutral state but stays in an isolated non-bonding configuration in the unpaired spin negative state. The system is then unfortunately a deep acceptor. This agrees with Petretto and Bruneval's study [20]. The spin density in this case is rather similar to that of the Zn-vacancy for which we found good agreement for the  $g$ -tensor with early experimental data by Galland and

Herve [43] characterized by a positive  $\Delta g_{\perp}$ -tensor where perpendicular means perpendicular to the dangling bond. For the interstitial sites, no levels in the gap are obtained and hence no spin density is observed unless we remove an electron from the VBM which gives a very different  $g$ -tensor. For the simple substitutional  $N_O$  we also found a  $g$ -tensor in reasonable agreement with experiment assuming that the experiment sees an average over different possible orientations of the N- $p$  orbital on which the spin is localized. These results suggest that further experimental work on these EPR centers, possibly with higher microwave frequency and magnetic field could help to resolve the individual centers with different orientation of the spin density.

Good agreement with experiment is also obtained for the hyperfine parameters both in the isolated molecules and for the  $N_2$  molecule on the O site and for the  $N_O$  substitutional case. We also provided hyperfine parameters for the  $V_{Zn}$  where we find notable hyperfine parameters only on the three nearest neighbor Zn to the O on which the electron spin is localized.

#### ACKNOWLEDGMENTS

We thank Davide Ceresoli and Dmitri Skachkov for useful discussions. K.D. was supported by the National Research Council of Thailand (NRCT), Grant No. NRCT5-RGJ63002-028. A.B. has been funded by National Research Council of Thailand (NRCT; 153/2564). W. R. L. L was supported by the U.S. Department of Energy Basic Energy Sciences (DOE-BES) under Grant No. DE-SC0008933. The calculations were performed at the Ohio Supercomputer Center.

- 
- [1] F. Mauri and S. G. Louie, Magnetic Susceptibility of Insulators from First Principles, *Phys. Rev. Lett.* **76**, 4246 (1996).
  - [2] F. Mauri, B. G. Pfommer, and S. G. Louie, Ab initio NMR Chemical Shift of Diamond, Chemical-Vapor-Deposited Diamond, and Amorphous Carbon, *Phys. Rev. Lett.* **79**, 2340 (1997).
  - [3] D. Skachkov, M. Krykunov, E. Kadantsev, and T. Ziegler, The Calculation of NMR Chemical Shifts in Periodic Systems Based on Gauge Including Atomic Orbitals and Density Functional Theory, *Journal of Chemical Theory and Computation* **6**, 1650 (2010), pMID: 26615697.
  - [4] E. S. Kadantsev and T. Ziegler, Implementation of a DFT-Based Method for the Calculation of the Zeeman  $g$ -Tensor in Periodic Systems with the Use of Numerical and Slater-Type Atomic Orbitals, *The Journal of Physical Chemistry A* **113**, 1327 (2009), pMID: 19173640.
  - [5] C. J. Pickard and F. Mauri, All-electron magnetic response with pseudopotentials: NMR chemical shifts, *Phys. Rev. B* **63**, 245101 (2001).
  - [6] C. J. Pickard and F. Mauri, First-Principles Theory of the EPR  $g$  Tensor in Solids: Defects in Quartz, *Phys. Rev. Lett.* **88**, 086403 (2002).
  - [7] D. Ceresoli, U. Gerstmann, A. P. Seitsonen, and F. Mauri, First-principles theory of orbital magnetization, *Phys. Rev. B* **81**, 060409 (2010).
  - [8] E. Rauls, E. N. Kalabukhova, S. Greulich-Weber, U. Gerstmann, D. Savchenko, A. Pöpl, and F. Mauri, Nitrogen Donor Aggregation in 4H-SiC:  $g$ -Tensor Calculations, in *Silicon Carbide and Related Materials 2006*, Materials Science Forum, Vol. 556 (Trans Tech Publications, 2007) pp. 391–394.
  - [9] U. Gerstmann, M. Rohrmüller, F. Mauri, and W. Schmidt, Ab initio  $g$ -tensor calculation for paramagnetic surface states: hydrogen adsorption at Si surfaces, *Physica Status Solidi (c)* **7**, 157 (2010).
  - [10] G. Pfanner, C. Freysoldt, J. Neugebauer, and U. Gerstmann, Ab initio epr parameters for dangling-bond defect complexes in silicon: Effect of jahn-teller distortion, *Phys. Rev. B* **85**, 195202 (2012).
  - [11] D. Skachkov, W. R. L. Lambrecht, H. J. von Bardeleben,

- U. Gerstmann, Q. D. Ho, and P. Deák, Computational identification of Ga-vacancy related electron paramagnetic resonance centers in  $\beta$ -Ga<sub>2</sub>O<sub>3</sub>, *Journal of Applied Physics* **125**, 185701 (2019).
- [12] D. Skachkov and W. R. L. Lambrecht, Computational study of electron paramagnetic resonance parameters for Mg and Zn impurities in  $\beta$ -Ga<sub>2</sub>O<sub>3</sub>, *Applied Physics Letters* **114**, 202102 (2019).
- [13] D. Skachkov, W. R. L. Lambrecht, K. Dabsamut, and A. Boonchun, Computational study of electron paramagnetic resonance spectra for Li and Ga vacancies in LiGaO<sub>2</sub>, *Journal of Physics D: Applied Physics* **53**, 17LT01 (2020).
- [14] N. Y. Garces, L. Wang, N. C. Giles, L. E. Halliburton, G. Cantwell, and D. B. Eason, Molecular nitrogen (N<sub>2</sub>-) acceptors and isolated nitrogen (N-) acceptors in ZnO crystals, *Journal of Applied Physics* **94**, 519 (2003).
- [15] W. R. L. Lambrecht and A. Boonchun, Identification of a N-related shallow acceptor and electron paramagnetic resonance center in ZnO: N<sub>2</sub><sup>+</sup> on the Zn site, *Phys. Rev. B* **87**, 195207 (2013).
- [16] P. J. Bruna and F. Grein, The A<sup>2</sup>Π<sub>u</sub> state of N<sub>2</sub><sup>+</sup>: Electric properties, fine and hyperfine coupling constants, and magnetic moments (g-factors). A theoretical study, *Journal of Molecular Spectroscopy* **250**, 75 (2008).
- [17] F. Napoli, M. Chiesa, E. Giamello, M. Fittipaldi, C. Di Valentin, F. Gallino, and G. Pacchioni, N<sub>2</sub>- Radical Anions Trapped in Bulk Polycrystalline MgO, *The Journal of Physical Chemistry C* **114**, 5187 (2010).
- [18] J. G. Reynolds, C. L. Reynolds, A. Mohanta, J. F. Muth, J. E. Rowe, H. O. Everitt, and D. E. Aspnes, Shallow acceptor complexes in p-type ZnO, *Applied Physics Letters* **102**, 152114 (2013).
- [19] J. G. Reynolds and C. L. Reynolds, Progress in ZnO Acceptor Doping: What Is the Best Strategy?, *Advances in Condensed Matter Physics* **2014**, 457058 (2014).
- [20] G. Petretto and F. Bruneval, Comprehensive Ab Initio Study of Doping in Bulk ZnO with Group-V Elements, *Phys. Rev. Applied* **1**, 024005 (2014).
- [21] N. H. Nickel and M. A. Gluba, Defects in Compound Semiconductors Caused by Molecular Nitrogen, *Phys. Rev. Lett.* **103**, 145501 (2009).
- [22] J. M. Philipps, J. E. Stehr, I. Buyanova, M. C. Tarun, M. D. McCluskey, B. K. Meyer, and D. M. Hofmann, Recharging behavior of nitrogen-centers in ZnO, *Journal of Applied Physics* **116**, 063701 (2014).
- [23] J. Heyd, G. E. Scuseria, and M. Ernzerhof, Hybrid functionals based on a screened Coulomb potential, *J. Chem. Phys.* **118**, 8207 (2003).
- [24] J. Heyd, G. E. Scuseria, and M. Ernzerhof, Erratum: "Hybrid functionals based on a screened Coulomb potential" [*J. Chem. Phys.* **118**, 8207 (2003)], *J. Chem. Phys.* **124**, 219906 (2006).
- [25] <https://www.vasp.at/>.
- [26] G. Kresse and J. Furthmüller, Efficiency of ab-initio total energy calculations for metals and semiconductors using a plane-wave basis set, *Computational Materials Science* **6**, 15 (1996).
- [27] G. Kresse and J. Hafner, Norm-conserving and ultrasoft pseudopotentials for first-row and transition elements, *Journal of Physics: Condensed Matter* **6**, 8245 (1994).
- [28] G. Kresse and D. Joubert, From ultrasoft pseudopotentials to the projector augmented-wave method, *Phys. Rev. B* **59**, 1758 (1999).
- [29] P. E. Blöchl, Projector augmented-wave method, *Phys. Rev. B* **50**, 17953 (1994).
- [30] P. Giannozzi, S. Baroni, N. Bonini, M. Calandra, R. Car, C. Cavazzoni, D. Ceresoli, G. L. Chiarotti, M. Cococcioni, I. Dabo, A. Dal Corso, S. de Gironcoli, S. Fabris, G. Fratesi, R. Gebauer, U. Gerstmann, C. Gougoussis, A. Kokalj, M. Lazzeri, L. Martin-Samos, N. Marzari, F. Mauri, R. Mazzarello, S. Paolini, A. Pasquarello, L. Paulatto, C. Sbraccia, S. Scandolo, G. Sciauzero, A. P. Seitsonen, A. Smogunov, P. Umari, and R. M. Wentzcovitch, Quantum espresso: a modular and open-source software project for quantum simulations of materials, *Journal of Physics: Condensed Matter* **21**, 395502 (19pp) (2009).
- [31] J. P. Perdew, K. Burke, and M. Ernzerhof, Generalized Gradient Approximation Made Simple, *Phys. Rev. Lett.* **77**, 3865 (1996).
- [32] P. Mori-Sánchez, A. J. Cohen, and W. Yang, Many-electron self-interaction error in approximate density functionals, *The Journal of Chemical Physics* **125**, 201102 (2006).
- [33] M. Cococcioni and S. de Gironcoli, Linear response approach to the calculation of the effective interaction parameters in the LDA + U method, *Phys. Rev. B* **71**, 035105 (2005).
- [34] I. Dabo, A. Ferretti, N. Poilvert, Y. Li, N. Marzari, and M. Cococcioni, Koopmans' condition for density-functional theory, *Phys. Rev. B* **82**, 115121 (2010).
- [35] S. Lany and A. Zunger, Generalized Koopmans density functional calculations reveal the deep acceptor state of N<sub>O</sub> in ZnO, *Phys. Rev. B* **81**, 205209 (2010).
- [36] See Supplementary Material at this paper's website for tests on Koopman's theorem, structural details and transition levels.
- [37] C. Freysoldt, B. Grabowski, T. Hickel, J. Neugebauer, G. Kresse, A. Janotti, and C. G. Van de Walle, First-principles calculations for point defects in solids, *Rev. Mod. Phys.* **86**, 253 (2014).
- [38] C. G. Van de Walle and P. E. Blöchl, First-principles calculations of hyperfine parameters, *Phys. Rev. B* **47**, 4244 (1993).
- [39] E. van Lenthe, E. J. Baerends, and J. G. Snijders, Relativistic regular two-component Hamiltonians, *The Journal of Chemical Physics* **99**, 4597 (1993), <http://dx.doi.org/10.1063/1.466059>.
- [40] E. van Lenthe, E. J. Baerends, and J. G. Snijders, Relativistic total energy using regular approximations, *The Journal of Chemical Physics* **101**, 9783 (1994), <http://dx.doi.org/10.1063/1.467943>.
- [41] T. Scholl, R. Holt, and S. Rosner, Fine and Hyperfine Structure in <sup>14</sup>N<sub>2</sub><sup>+</sup>: The B<sup>2</sup>Σ<sub>u</sub><sup>+</sup>-X<sup>2</sup>Σ<sub>g</sub><sup>+</sup>(0,0) Band, *Journal of Molecular Spectroscopy* **192**, 424 (1998).
- [42] L. B. Knight, J. M. Bostick, R. W. Woodward, and J. Steadman, An electron bombardment procedure for generating cation and neutral radicals in solid neon matrices at 4 K: ESR study of <sup>14</sup>N<sub>2</sub><sup>+</sup> and <sup>15</sup>N<sub>2</sub><sup>+</sup>, *The Journal of Chemical Physics* **78**, 6415 (1983).
- [43] D. Galland and A. Herve, ESR spectra of the zinc vacancy in ZnO, *Physics Letters A* **33**, 1 (1970).
- [44] N. T. Son, J. Isoya, I. G. Ivanov, T. Ohshima, and E. Janzén, Magnetic resonance identification of hydrogen at a zinc vacancy in ZnO, *Journal of Physics: Condensed Matter* **25**, 335804 (2013).
- [45] Y. Frodason, K. Johansen, T. Bjørheim, B. Svensson,

- and A. Alkauskas, Zn vacancy as a polaronic hole trap in zno, *Physical Review B* **95**, 094105 (2017).
- [46] Y. Frodason, K. Johansen, T. Bjørheim, B. Svensson, and A. Alkauskas, Zn vacancy-donor impurity complexes in zno, *Physical Review B* **97**, 104109 (2018).
  - [47] J. Bang, Y.-Y. Sun, D. West, B. K. Meyer, and S. Zhang, Molecular doping of zno by ammonia: a possible shallow acceptor, *Journal of Materials Chemistry C* **3**, 339 (2015).
  - [48] A. Kohan, G. Ceder, D. Morgan, and C. G. Van de Walle, First-principles study of native point defects in zno, *Physical Review B* **61**, 15019 (2000).
  - [49] P. Erhart, K. Albe, and A. Klein, First-principles study of intrinsic point defects in zno: Role of band structure, volume relaxation, and finite-size effects, *Physical Review B* **73**, 205203 (2006).
  - [50] J. L. Lyons, A. Janotti, and C. G. Van de Walle, Why nitrogen cannot lead to p-type conductivity in ZnO, *Applied Physics Letters* **95**, 252105 (2009).
  - [51] C. Park, S. Zhang, and S.-H. Wei, Origin of p-type doping difficulty in zno: The impurity perspective, *Physical Review B* **66**, 073202 (2002).
  - [52] S. Falletta, J. Wiktor, and A. Pasquarello, Finite-size corrections of defect energy levels involving ionic polarization, *Phys. Rev. B* **102**, 041115 (2020).
  - [53] W. R. L. Lambrecht, A. V. Rodina, S. Limpijumnong, B. Segall, and B. K. Meyer, Valence-band ordering and magneto-optic exciton fine structure in ZnO, *Phys. Rev. B* **65**, 075207 (2002).